ACS NANO

www.acsnano.org

ARTICLE

pH-Controlled Detachable DNA Circuitry and Its Application in Resettable Self-Assembly of Spherical Nucleic Acids

Yijun Guo,[#] Dongbao Yao,[*,#] Bin Zheng, Xianbao Sun, Xiang Zhou, Bing Wei, Shiyan Xiao, Miao He, Chengxu Li, and Haojun Liang[*]

Cite This: *ACS Nano* 2020, 14, 8317−8327

Read Online

ACCESS | Metrics & More | Article Recommendations | Supporting Information

ABSTRACT: Toehold-mediated strand displacement reaction, the fundamental basis in dynamic DNA nanotechnology, has proven its extraordinary power in programming dynamic molecular systems. Programmed activation of the toehold in a DNA substrate is crucial for building sophisticated DNA devices with digital and dynamic behaviors. Here we developed a detachable DNA circuit by embedding a pH-controlled intermolecular triplex between the toehold and branch migration domain of the traditional "linear substrate". The reaction rate and the "on/off" state of the detachable circuit can be regulated by varying the pHs. Similarly, a two-input circuit composed of three pH-responsive DNA modules was then constructed. Most importantly, a resettable self-assembly system of spherical nucleic acids was built by utilizing the high detachability of the intermolecular triplex structure-based DNA circuit. This work demonstrated a dynamic DNA device that can be repeatedly operated at constant temperature without generating additional waste DNA products. Moreover, this strategy showed an example of recycling waste spherical nucleic acids from a self-assembly system of spherical nucleic acids. Our strategy will provide a facile approach for dynamic regulation of complex molecular systems and reprogrammable nanoparticle assembly structures.

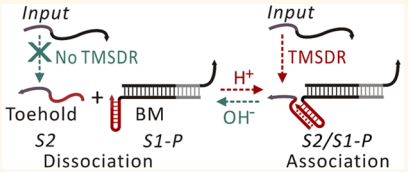

KEYWORDS: *detachable DNA circuit, intermolecular triplex, pH-responsive, resettable self-assembly, spherical nucleic acids*

DNA has been employed as a versatile building block for the fabrication of those molecular systems with precise nanostructures due to its distinct programmability and predictability.[1,2] The toehold-mediated strand displacement reaction (TMSDR),[3] a process wherein an invading strand binds with a complementary single-stranded domain (called toehold) on a DNA substrate and then displaces one or two prehybridized strands through branch migration (BM), provides a powerful programmable approach in constructing sophisticated molecular systems with dynamic behaviors in the field of dynamic DNA nanotechnology.[4,5] Diverse dynamic nanodevices with a variety of functions that derive from the principle of strand displacement have included DNA molecular gears,[6] catalytic networks for signal amplification,[7,8] large-scale digital DNA circuits with algorithmic behaviors,[9,10] DNA walkers that move along well-designed tracks,[11−14] logical assembly of nanoparticles,[15] autonomous oscillators,[16] and single-molecule DNA navigators.[17]

The crucial factor in building these dynamic molecular systems is the programmed activation of the toehold sequestered in a DNA substrate; that is, bonds between DNA strands are needed to be controllably made and broken through TMSDRs.[18−20] Recently, some alternative approaches for toehold activation, including remote toehold modulation,[18] associative toehold activation,[19] allosteric DNA toehold design,[20] and intramolecular conformational motion strategy,[21] have been developed to expand the toolbox of TMSDR techniques. However, these strategies still have several drawbacks, which will limit the construction of more complex and robust dynamic DNA systems. For example, the introduced DNA spacer between the toehold and BM domain in the remote toehold strategy potentially complicates the design rules for constructing complex dynamic DNA systems.[18] In addition, using the approach, an additional external factor almost cannot be employed to dynamically regulate the DNA circuit once the input strand is added. Although other strategies can improve the dynamic regulation abilities of TMSDRs, those introduced additional reactants lead to production of many waste DNA complexes, which are

Received: March 18, 2020
Accepted: June 24, 2020
Published: June 24, 2020

https://dx.doi.org/10.1021/acsnano.0c02329
ACS Nano 2020, 14, 8317−8327

also not conducive to the construction of complex DNA networks.[19−21]

Therefore, it is worthwhile to create a more facile regulation approach for toehold activation to implement the programmable dynamic control of the TMSDR-based DNA circuit. A pH-responsive CG-C$^+$ triplex DNA structure,[22] composed of a cytosine-rich single-stranded DNA (called the triplex-forming strand) and a CG duplex through Hoogsteen interactions (average pK_a of cytosines in triplex DNA is ∼6.5),[23] has been recently applied to shape-memory DNA hydrogels,[24,25] drug delivery,[26] and pH-responsive self-assembly of DNA nanostructures.[27−30] Inspired by the well-established triplex DNA structure with high conformation reversibility and our previous "junction substrate" structure (assembled by complementary short double-stranded DNA motifs),[31] herein we create a "detachable substrate"-based DNA circuit by embedding an intermolecular triplex DNA structure into the connection point between the toehold and the BM domain of the traditional "linear substrate" (Figure S1). The proposed "detachable substrate" of the DNA circuit consists of two pH-responsive modules that can be reversibly associated/dissociated through the formation/destruction of the pH-responsive triplex DNA structure in a programmable way.

RESULTS AND DISCUSSION

Construction Principle of pH-Controlled Detachable DNA Circuit. A typical reaction scheme for the pH-controlled detachable DNA circuit is shown in Figure 1. In acidic condition (pH 5.5), the hairpin domain (2-2*) in the BM module (S1-P) and domain 2** in the toehold module (S2) can assemble into an intermolecular CG-C$^+$ triplex structure through Hoogsteen interactions; thus these two modules are connected together to form a complete substrate. Upon addition of the input strand, the domain 1* of input binds with its complementary toehold (domain 1) in S2 to initiate the TMSDR to displace the prehybridized protector strand P in S1-P into solution while generating a waste complex W (analogous to a three-way junction structure) composed of the strands S1, S2, and input. The exposed domain 4* in the released P can then interact with the fluorescent reporter R (formed by a fluorophore strand F labeled with a pH-insensitive dye Cy5[32] and a corresponding quencher strand Q) to generate fluorescence signal through the TMSDR. In contrast, at pH 7.0 (neutral condition), the destruction of the intermolecular CG-C$^+$ triplex structure leads to the separation of S1-P and S2, which prevents the TMSDR from happening in the presence of the input strand.

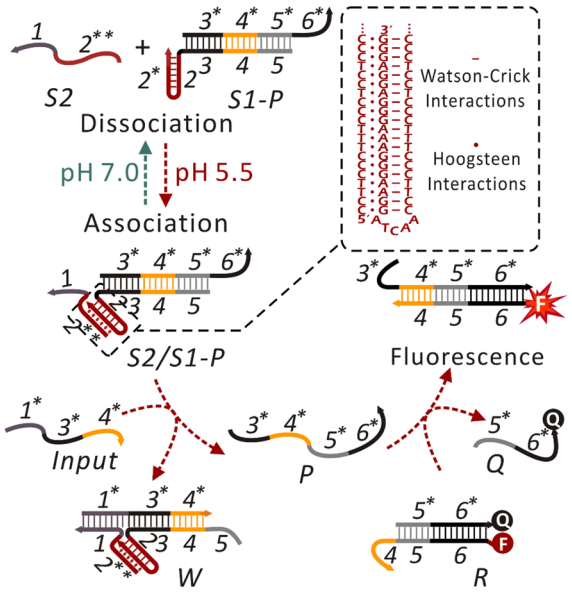

Figure 1. Graphical representation of the intermolecular CG-C$^+$ triplex structure-based pH-controlled DNA circuit.

Operation of pH-Controlled Detachable DNA Circuit. We first optimized the reaction condition of the DNA circuit at pH 5.5 by varying the concentration of S2 (from 0 to 400 nM) with the addition of fixed concentrations of S1-P (200 nM) and input (600 nM). The reaction rate increased with the increase of the concentration of S2 from the real-time fluorescence kinetic curves (Figure S3). Hence, in order to ensure the reaction sensitivity of the system, the concentrations of S1-P and S2 were determined as 200 and 400 nM, respectively. The pH-responsiveness of the CG-C$^+$ triplex DNA-based "detachable substrate" was confirmed through the characterization of native polyacrylamide gel electrophoresis (PAGE) at pH 5.5 and 7.0, respectively. As shown in Figure S4, the substrate (S2/S1-P) and the produced complex W (S2/S1-input) can form only under acidic condition (pH 5.5).

Then, the performance of the pH-controlled DNA circuit was investigated at pH 5.5 in the presence of different concentrations of input. As expected, a significant increase of the TMSDR rate was observed when the input concentration was increased from 0 to 600 nM (Figure 2a), accompanied by the increase in input consumption in the system (from 0 to 200 nM) after 2.5 h of reaction (Figure S5). In contrast, almost no fluorescent signal was observed at pH 7.0 because the TMSDR cannot proceed when S1-P and S2 are separated (Figure 2b). A detailed analysis of the pH-dependence for the detachable DNA circuit was performed by fixing the concentration of input at 400 nM. It can be found that the activation level of the TMSDR can be effectively regulated at different pHs (Figure 2c), indicating the gradual formation of the intermolecular triplex structure with the decrease of pH (from pH 7.0 to 5.5). In addition, the corresponding pH-dependent curve obtained from the end points in Figure 2c also demonstrated the gradual activation of the TMSDR can be achieved by gradually decreasing the pH value of the solution (Figure 2d). In contrast, a series of control experiments involving a pH-insensitive circuit (domain 2** in S2 was substituted with a random DNA sequence which is unable to interact with S1-P at acidic pH, Figure S6a) indicated that the TMSDR cannot be activated with any concentration of the input strand added (lines from 0 to 600 nM at pH 5.5 in Figure S6b) and at any pH explored (lines from pH 5.5 to 7.0 in Figure S6c) due to the inability to form an intermolecular CG-C$^+$ triplex DNA-based substrate (lane 10 of the PAGE gel image in Figure S4a).

Dynamic Programming of pH-Controlled Detachable DNA Circuit. Considering that the most notable feature of the triplex structure is the high conformation reversibility,[22,30] the "on/off" state of the TMSDR in the pH-controlled DNA circuit should be able to be dynamically regulated due to the fact that S1-P and S2 can be reversibly associated/dissociated through cyclic pH changes (Figure 3a). To demonstrate the dynamic programming of the TMSDR, the pH of the solution was cyclically varied between 5.5 and 7.0 and the concentration of input was fixed at 400 nM. As shown in Figure 3b, the

https://dx.doi.org/10.1021/acsnano.0c02329
ACS Nano 2020, 14, 8317−8327

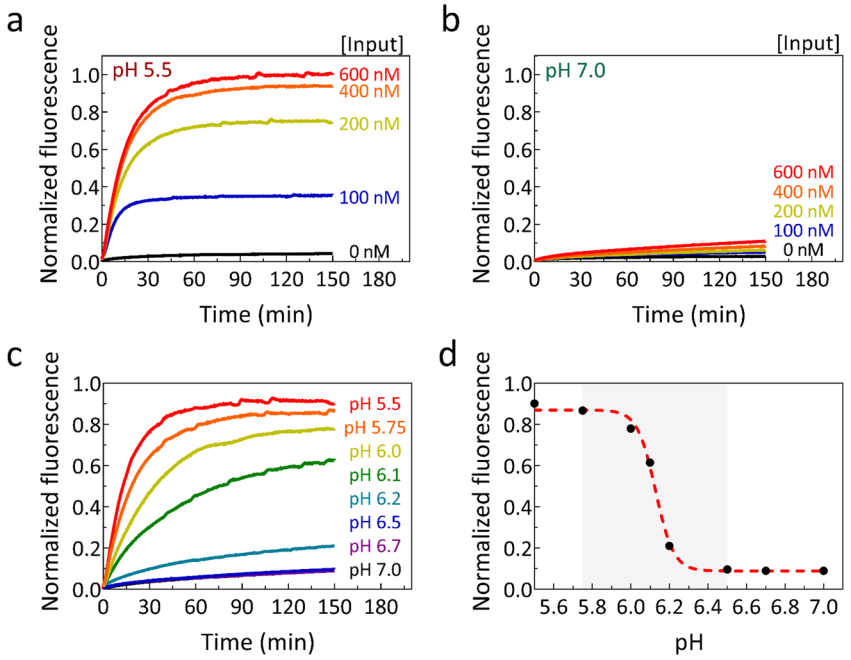

Figure 2. Real-time fluorescence kinetics of the pH-controlled DNA circuit under varied concentrations of the input strand at pH 5.5 (a) and pH 7.0 (b), respectively. (c) The pH dependence of the TMSDR rate of the pH-controlled DNA circuit in the presence of 400 nM input can be finely regulated at different pHs. (d) Corresponding fitted pH-dependent curve after 2.5 h of reaction. The experiments were performed at 37 °C, [S1-P] = 200 nM, [S2] = 400 nM, [R] = 250 nM.

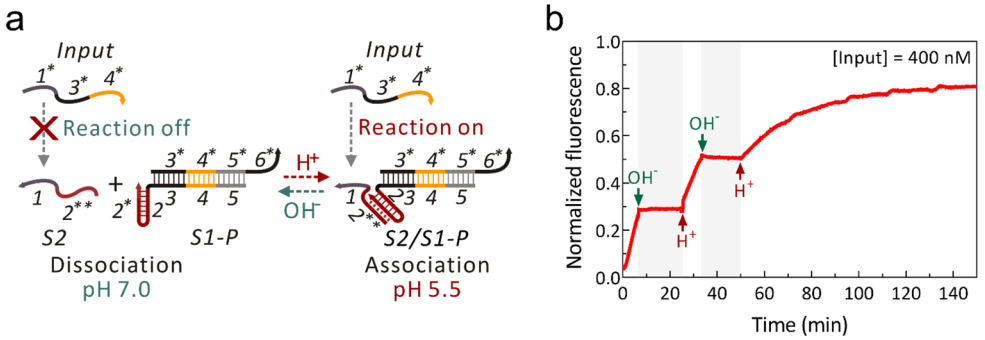

Figure 3. (a) Schematic of the programmable "on/off" state of the TMSDR of the pH-controlled DNA circuit. (b) Real-time changes of the fluorescent signal in response to the cyclic variations of the pH between 5.5 and 7.0 by adding small aliquots of 0.5 M HCl or NaOH. The experiment was performed at 37 °C, [S1-P] = 200 nM, [S2] = 400 nM, [input] = 400 nM, [R] = 250 nM.

TMSDR between substrate (S2/S1-P) and input was completely inhibited when the pH of the solution was altered from 5.5 to 7.0, and the TMSDR was turned on again after the pH was tuned back to 5.5. Therefore, the association/dissociation of the "detachable substrate" composed of two pH-responsive modules can be precisely controlled by dynamic pH changes in a programmable way. Compared with the allosteric toehold strategy[20] and the intramolecular conformational motion strategy,[21] where the dynamic control of the TMSDR was achieved by the introduction of additional DNA strands accompanied by the production of a large number of DNA waste complexes, our pH-controlled strategy allows more facile regulation of the TMSDR by adding only small aliquots of HCl or NaOH without producing DNA waste complexes. In addition, our strategy is easier to employ in the construction and dynamic regulation of complex DNA networks due to the fact that the pH-responsive intermolecular triplex structure does not participate in the TMSDR process, but only serves to connect the reactants.

pH-Controlled Two-Input DNA Circuit. The advancement of the toehold-mediated strand displacement principle allows the development of highly complex DNA circuits and sophisticated DNA devices.[33−37] To further demonstrate the flexibility and adaptability of our pH-responsive intermolecular triplex structure-based strategy in the programming of more complex DNA circuits, we wanted to design a pH-controlled two-input circuit composed of more pH-responsive DNA modules. To this end, we first constructed another pH-controlled single-input DNA circuit by substituting the CG-C$^+$ triplex structure with a TA-T triplex structure that is stable at neutral pH (Figure S7). Compared with the CG-C$^+$ triplex DNA, the TA-T triplex DNA dissociates into TA duplexes and a single-stranded domain at much higher pHs due to the deprotonation pK_a of thymine being ~10.[22] The intermolecular TA-T triplex structure-based DNA circuit can be activated at pH 7.0 and was completely turned off at pH 10.0 due to the destruction of the TA-T triplex structure (Figure S8). Similarly, the activation level of the TA-T triplex structure-

https://dx.doi.org/10.1021/acsnano.0c02329
ACS Nano 2020, 14, 8317−8327

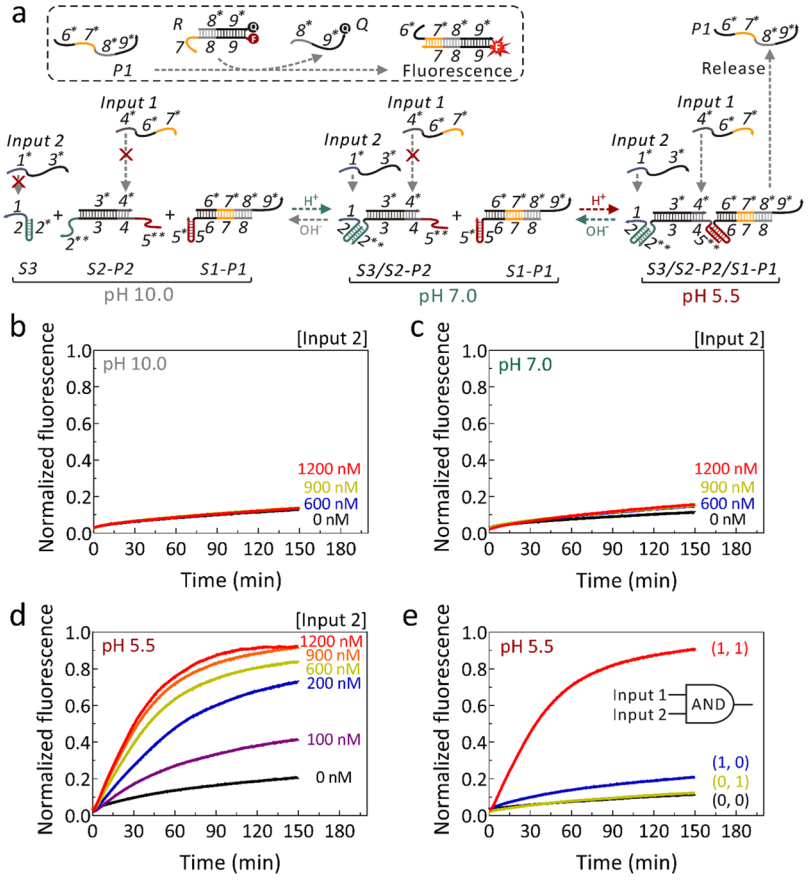

Figure 4. (a) Brief scheme for the pH-controlled two-input DNA circuit. A more detailed reaction mechanism can be found in Figure S10. (b–d) Real-time fluorescence kinetics for the TMSDRs in the pH-controlled two-input DNA circuit in the presence of different amounts of input 2 at pH 10.0, 7.0, and 5.5, respectively. The concentration of input 1 was fixed at 600 nM. (e) Fluorescent signal outputs of the constructed AND gate at pH 5.5, [input 1] = 600 nM, [input 2] = 900 nM. All kinetic experiments were performed at 37 °C, [S1-P1] = 200 nM, [S2-P2] = 600 nM, [S3] = 600 nM, [R] = 250 nM.

based DNA circuit can also be regulated through gradually varying the pH of the solution from 7.0 to 10.0 (Figure S9).

As depicted in Figure 4a, we then designed a pH-controlled two-input DNA circuit by integrating the CG-C$^+$ triplex structure-based DNA circuit with the TA-T triplex structure-based DNA circuit (a more detailed version of the scheme can be found in Figure S10). The substrate of the two-input DNA circuit consists of three modules: (i) S1-P1 (formed by hybridization of S1 and P1), S2-P2 (composed of S2 and P2), and a hairpin structure-based toehold S3. At pH 10.0, these three separated modules are unable to assemble into an integrated substrate due to the inability for the formation of any triplex structure. If the pH is altered from 10.0 to 7.0, the hairpin domain (2-2*) in S3 can associate with its corresponding triplex-forming domain (2**) in S2-P2 through Hoogsteen interactions to form a TA-T triplex structure-based DNA complex, S3/S2-P2. Although input 2 can bind with the toehold (domain 1) on S3 and displace the strand P2 that is prehybridized with S2 through the TMSDR to generate a new toehold (domain 4) that is complementary with input 1, the separated S1-P1 will not lead to the TMSDR between input 1 and S1-P1. Only if the pH of the solution decreases to 5.5 can these three DNA modules assemble into the complete two-arm substrate (S3/S2-P2/S1-P1) through Hoogsteen interactions to initiate the cascade TMSDRs between input 1, input 2, and S3/S2-P2/S1-P1 to release the final product P1. The released P1 then binds with the pH-insensitive reporter R to generate fluorescent signal through another TMSDR.

We first determined the ratio of S1-P1 to S2-P2 to S3 as 1:3:3 after the optimization of the reaction condition of the pH-responsive two-input DNA circuit at pH 5.5 (Figure S11). Then, the performance of the two-input DNA circuit was investigated at pH 10.0, 7.0, and 5.5, respectively (Figure 4b–d). An excess amount of input 1 (600 nM) and different concentrations of input 2 were added to observe the responsiveness of the two-input system. As expected, no obvious fluorescent signals were produced at pH 10.0 (Figure 4b) and 7.0 (Figure 4c) due to the inability for the formation of the complete substrate, while at pH 5.5, the fluorescence intensity increased obviously with the increase of the added input 2 (from 0 to 1200 nM), indicating the complete formation of the two-arm substrate and the occurrence of the cascade TMSDRs. Moreover, the pH-responsive two-input DNA circuit implemented a good Boolean logic function (AND logic gate) at pH 5.5; that is, the two-input DNA circuit was triggered only in the presence of both input 1 and input 2 (Figure 4e).

Fixing the concentration of input 1 at 600 nM and the concentration of input 2 at 900 nM, a more detailed analysis of the pH-dependence for the activation level of the two-input DNA circuit was performed by gradually decreasing the pH of the solution from 10.0 to 5.5 (Figure S12). The two-input DNA circuit always remained in an "off" state when the pH

https://dx.doi.org/10.1021/acsnano.0c02329
ACS Nano 2020, 14, 8317–8327

varied from 10.0 to 7.0 due to the fact that the assembly of S1 and S2-P2 was unable to be triggered over this pH window, whereas the activation level of the two-input DNA circuit started to gradually increase when the pH decreased from 7.0 to 5.5, suggesting the gradual formation of the two-arm substrate assembled by S1-P1, S2-P2, and S3 through Hoogsteen interactions (Figure S12). As a control experiment, a pH-independent substrate-based two-input system was designed, and no fluorescent signal was observed when the pH decreased from 10.0 to 5.5 (Figure S13).

Design Principle of pH-Controlled Resettable Self-Assembly of Spherical Nucleic Acids. TMSDR provides a powerful engineering approach for programming a wide variety of dynamic DNA devices under nonequilibrium conditions. However, reverting to their original states through external stimulations (*e.g.*, heat or electricity) usually is not possible for these TMSDR-based molecular systems once equilibriums are reached, except by cumbersome and nonrobust fluid mixing or exchange.[38] Although some dynamic molecular systems can be refueled for repeated operations after addition of extra DNA strands, the accumulation of generated DNA wastes and byproducts causes degradation of their performances and wasting of materials.[3,39] Recently, Hahn and Shih reported a temperature-dependent associative TMSDR-based DNA circuit that can be repeatedly operated *via* thermal cycling.[40] However, their strategy needs to be realized by precisely altering the reaction temperature with the assistance of specialized thermal cyclers, which severely handicaps its possible applications in isothermal conditions and living systems. To overcome these drawbacks, it is really essential to develop a facile TMSDR-based DNA dynamic system that can be repeatedly operated at constant temperature without generating any DNA waste products. The highly detachable nature of our pH-controlled intermolecular triplex structure-based DNA circuit provides the possibility to build this kind of resettable DNA devices.

A gold nanoparticle (AuNP) functionalized with a highly oriented nucleic acids shell, known as a spherical nucleic acid (SNA) possessing both a distinct optical property of the AuNP and powerful programmability of nucleic acids,[41] was reported by Mirkin *et al.* in the mid-1990s.[42] To date, SNAs have been widely employed in colloidal superlattice structures,[43−46] microRNA imaging,[47,48] colorimetric biosensors,[49−52] programmable and logical assembly nanostructures,[15,52−54] drug delivery,[26,55] and single nucleotide polymorphism (SNP) discrimination.[56,57]

Here we create a resettable SNA assembly system programmed by cyclic variations of pH through integrating the pH-controlled detachable DNA circuit with the self-assembly of SNAs. Inspired by the construction mechanism of the face-centered-cubic SNA superlattice,[43] only one type of SNA conjugate is employed in our design. As shown in the upper left corner of Figure 5, the resettable SNA assembly system comprises two pH-responsive modules: (i) an SNA conjugate named SNA-S2 formed by hybridization of an extended anchor domain on S2 (domain 1*) with its complementary domain (domain 1) on the SNA surface; (ii) a DNA complex (S1-P) with a self-complementary sticky end ($^{5'}$-TGCGCA$^{3'}$) at the 3′ end of S1, which is initially deactivated due to partial protection by protector P. These two modules can be reversibly associated and dissociated through the formation and destruction of the pH-responsive intermolecular CG-C$^+$ triplex DNA structure (formed by the triplex-forming domain (2**) on SNA-S2 and the hairpin domain (2-2*) of S1-P).

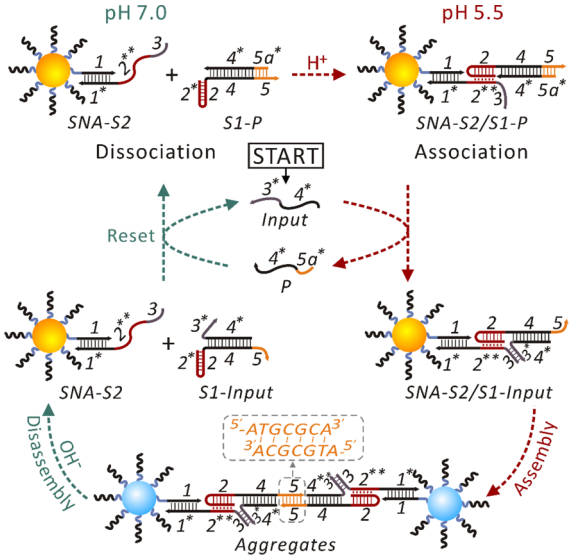

Figure 5. Schematic illustration of the resettable self-assembly system of spherical nucleic acids controlled by cyclic pH changes.

At pH 7.0, S1-P cannot associate with SNA-S2, yielding a stable system with dispersed SNA conjugates in the presence of input (Figure 5). Once the pH of the solution is tuned to 5.5, these two modules can be connected to form a new SNA conjugate (SNA-S2/S1-P) through Hoogsteen interactions. Then, domain 3* of the input strand binds with the forward invading toehold (domain 3) of S2 on the SNA surface and subsequently displaces P into solution to activate the protected sticky end through the TMSDR, accompanied by the production of a rigid three-way junction complex on the SNA surface (SNA-S2/S1-input). The activated self-complementary sticky ends on the SNA surface could interact with each other to form cross-link points through cooperative interactions to assemble SNA conjugates into visible aggregates. The entire SNA assembly process can be detected by UV−vis spectroscopy or through naked eye observation. If the pH is restored to 7.0 again, the intermolecular CG-C$^+$ triplex DNA structure will be destroyed immediately, resulting in the destruction of the rigid three-way junction complex (S2/S1-input). Then, domain 3* (composed of 9 bases) of the input will dissociate from the forward invading toehold (domain 3) on S2 due to the thermodynamic instability of the short duplex DNA; meanwhile, the cross-link point composed of only 6 base pairs also will be broken. Thus, S1-input will completely detach from the SNA surface, leading to the rapid disassembly of SNA conjugates. Afterward, since the forward invading toehold (domain 3) on S2 is not connected with S1-input at pH 7.0, domain 5a* (composed of 4 bases) of the released protector P will interact with the reverse toehold (domain 5) on S1-input to replace the input strand to form S1-P again through a new TMSDR. In this way, the pH-controlled SNA assembly system can be completely reset without generating any DNA waste products by dynamically changing the pH back to 7.0.

Repeated Operation of the pH-Controlled SNA Assembly System. We first started to optimize the experimental condition that enables the pH-controlled SNA assembly system. In order to ensure the sensitivity of the SNA

https://dx.doi.org/10.1021/acsnano.0c02329
ACS Nano 2020, 14, 8317−8327

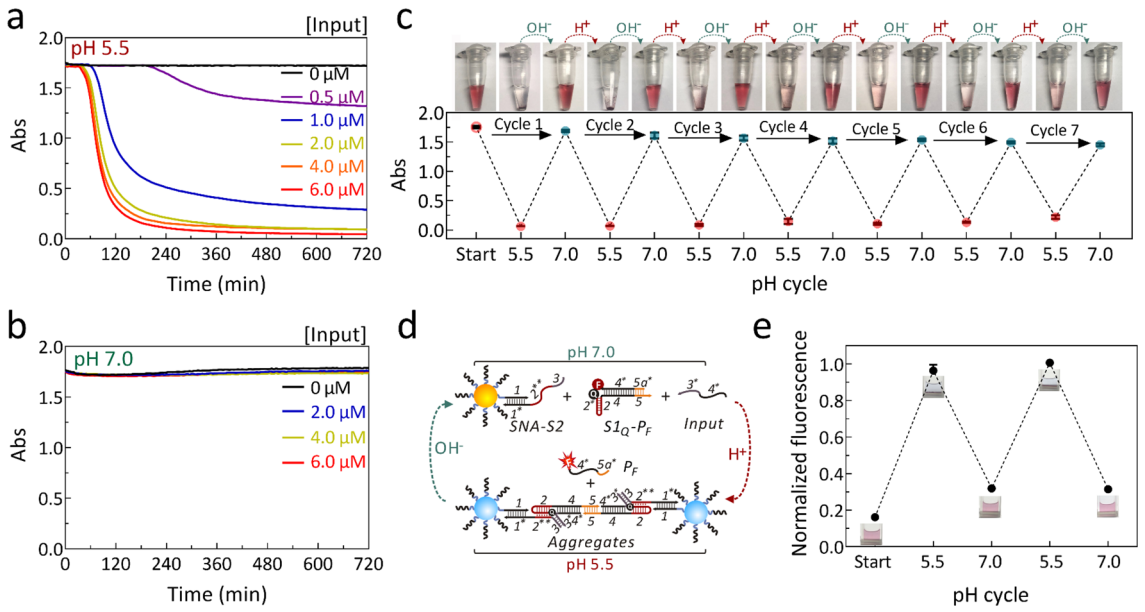

Figure 6. Kinetics of the SNA assembly with the addition of different concentrations of input at pH 5.5 (a) and pH 7.0 (b), respectively. (c) Color changes and the corresponding absorbance values at 520 nm of the supernatant of the SNA solution showing the ability of the pH-controlled SNA assembly system in repeated operation by cyclically varying the pH between 5.5 and 7.0 in the presence of 6 μM input. [S2] = 1 μM, [S1-P] = 2 μM, [SNA] = 20 nM. (d) The TMSDR process in the pH-controlled SNA assembly system can be tracked through the introduction of a pH-insensitive reporter. (e) Reversible fluorescent signal changes in the pH-controlled SNA assembly system when the pH was cyclically changed between 7.0 and 5.5. [S2] = 1 μM, [$S1_Q$-P_F] = 2 μM, [input] = 6 μM, [SNA] = 20 nM. All experiments were operated at 37 °C.

assembly reaction at pH 5.5, the molar ratio of S2 to SNA was determined as 50 (Figure S14). Then, we investigated the performance of the SNA assembly system in the presence of different concentrations of input at pH 5.5 *via* monitoring the real-time UV−vis absorption spectroscopy at 520 nm (Figure 6a). It was clearly seen that the SNA aggregation rate significantly accelerated with the increase of input concentration (from 0 to 6 μM), and the SNA conjugates could almost achieve an aggregation equilibrium in 4 h when the input concentration rose to 1 μM. The SNA conjugates were completely aggregated in 12 h when the input concentration rose to 2 μM, suggesting that the protected sticky ends on the SNA surface were fully activated through TMSDRs. In contrast, no aggregation was observed at pH 7.0 due to the fact that S1-P cannot associate with SNA-S1 (Figure 6b). A negative control experiment was then performed by dynamically changing the pH of the SNA solution between 5.5 and 7.0 to prove the SNA aggregation specificity of our pH-controlled SNA assembly system (Figure S15). In addition, at pH 5.5, our SNA assembly system exhibited excellent specificity in the discrimination of the correct input strand and those spurious input strands with single-base mismatch at different positions (Figure S16). Moreover, the pH-controlled SNA assembly system can be applied to more complex environments (Figures S17 and S18). As shown in Figure S17, the SNA conjugates exhibited good aggregation activity in the presence of as high as 2 M NaCl with the addition of 2 μM input at pH 5.5, while the system still showed good stability without the addition of input in 12 h. In addition, the pH-controlled SNA assembly system can also work in the reaction buffer containing 10% fetal bovine serum (Figure S18).

Then, the performance of the pH-controlled SNA assembly system for repeated operation was investigated through observation of visible color changes by cyclically altering the pH of the solution from 5.5 to 7.0. As shown from the color photos (upper panel of Figure 6c), upon addition of 6 μM input at pH 5.5, visible SNA aggregates were gradually deposited at the bottom of a 200 μL plastic tube after 12 h of reaction. Interestingly, the SNA aggregates were instantly disassembled into dispersed SNA conjugates after the pH was tuned to 7.0 (Video S1) due to the rapid destruction of the intermolecular triplex DNA structure (with a fast response time of less than 200 ms[22]) and the dissociation of S1-input from SNA aggregation networks. Notably, the sample was maintained at pH 7.0 for 1 h to enable the accomplishment of the reverse TMSDR between P and S1-input to reset the SNA assembly system. Then, visible aggregates were gradually formed again after the pH of the system was tuned back to 5.5. The color of the SNA solution at pH 7.0 was getting a little lighter after each reaction cycle (upper panel of Figure 6c) because the reaction volume (the initial volume was 60 μL) was slightly increasing after the repeated introduction of 0.5 M HCl and 0.5 M NaOH (0.75 μL each time). In addition, the corresponding absorbance value at 520 nm of the supernatant of the SNA solution after each change in pH value was measured by a UV−vis spectrophotometer (lower panel of Figure 6c). In order to further quantitatively analyze the reversibility of the aggregation/dispersion of the pH-controlled SNA assembly system, we defined the term "aggregation degree (AD)" as $AD = 1 - \frac{A(60 + 0.75 \times n)}{60 \times A_0}$ to characterize the aggregation level of the SNA conjugates at pH 5.5, where A_0, A, and n denote the absorbance value of the initial system (1.75), the absorbance value of the supernatant of the system after pH changes, and the number of pH changes, respectively. Similarly, the term "dispersion degree (DD)" was defined as $DD = \frac{A(60 + 0.75 \times n)}{60 \times A_0}$ to quantify the disassembly level of the SNA aggregates at pH 7.0. As shown in Figure S19a, there has

https://dx.doi.org/10.1021/acsnano.0c02329
ACS Nano 2020, 14, 8317−8327

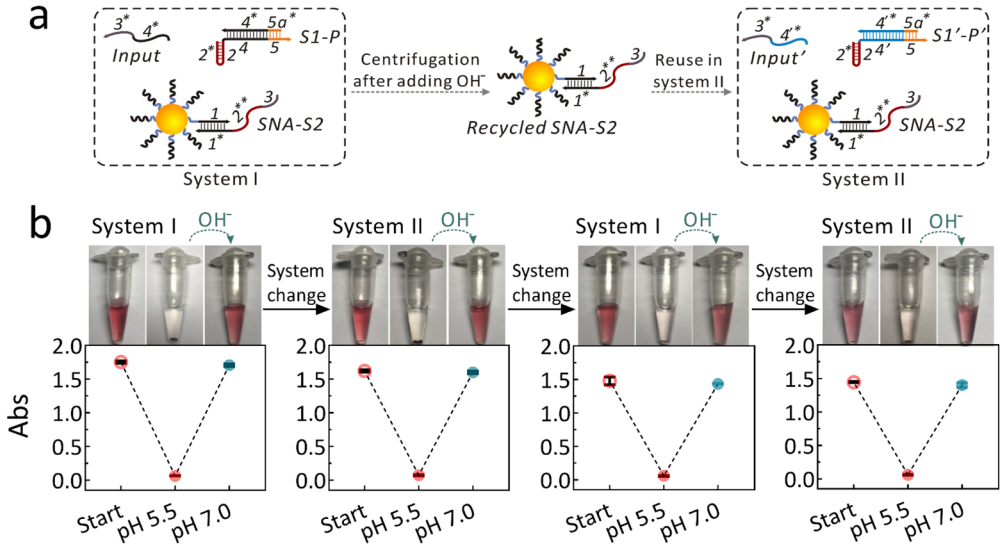

Figure 7. (a) Schematic showing the reuse process of the SNA conjugate in two pH-controlled SNA assembly systems. (b) Color images and the corresponding absorbance values at 520 nm of the supernatant of the SNA solution at different pH states during the reuse process of the recycled SNA-S2 in two pH-controlled SNA assembly systems at 37 °C. [S2] = 1 μM, [S1-P] = [S1′-P′] = 2 μM, [input] = [input′] = 6 μM, [SNA] = 20 nM.

been no apparent change for the value of AD from reaction cycle 1 to 6 (decreased from 0.963 to 0.915) until the number of cycles up to 7 (0.856), while the value of DD has been almost unchanged from cycle 1 to cycle 7 (decreased from 0.979 to 0.964), which indicated that there was no obvious irreversible loss of the SNA conjugates during the repetition (Figure S19b). As a consequence, the repeated operation of the SNA assembly system can proceed with negligible loss of reactivity for 6 pH shift cycles, which demonstrated the high dynamic programmability and reversibility of the pH-controlled detachable DNA circuit-based SNA assembly system.

To verify that the reverse TMSDR between S1-input and P indeed occurred after the SNA disassembly, a pH-insensitive fluorophore (Cy5) labeled at the 3′ end of P (named P_F) and an opposing quencher labeled at the 5′ end of S1 (named $S1_Q$) were introduced into the SNA assembly system to track the TMSDR process (Figure 6d). As shown in Figure 6e, both visible SNA aggregates and fluorescent signal were observed when the pH was altered from the initial 7.0 to 5.5 due to the release of P_F and activation of the SNA conjugate through TMSDR in acidic conditions. As expected, the fluorescent signal produced from the released P_F almost disappeared after 1 h of reaction when the pH was restored to 7.0 again, indicating that the occurrence of the reverse TMSDR between $S1_Q$-input and P_F led to the regeneration of $S1_Q$-P_F and input; that is, the pH-controlled SNA assembly was reset at pH 7.0.

Recycling of SNA Conjugates from a pH-Controlled SNA Assembly System. The synthesis of the SNA conjugate is a time-consuming and expensive process in the field of SNA assembly.[58] However, the SNA conjugates are very difficult to recycle after assembly due to the high specificity of DNA hybridization. The design of the detachable intermolecular triplex DNA adopted in the pH-controlled resettable SNA assembly system makes the recycling of the SNA conjugates possible for operation at constant temperature. As a demonstration, two pH-controlled SNA assembly systems (system I and system II) sharing the same SNA conjugate (SNA-S2) are employed in the recycling experiment of the SNA conjugate (Figure 7a). At an initial pH of 5.5, visible SNA aggregates were gradually formed at the bottom of a plastic tube after adding input into system I (upper panel of Figure 7b). The SNA aggregates rapidly disassembled into dispersed SNA conjugates by changing the pH to 7.0. Then, the SNA solution was centrifuged and redispersed in reaction buffer to obtain recycled SNA-S2. The recycled SNA-S2 was then reused in system II after addition of S1′-P′ and input′ under equal reaction volumes with system I (60 μL) at pH 5.5. With the same operation, the recycled SNA-S2 was reused three times between two SNA assembly systems (upper panel of Figure 7b). In addition, the corresponding absorbance value at 520 nm of the supernatant of the SNA solution at each pH state during the recycling experiment was measured (lower panel of Figure 7b). Similarly as above, the term "recycling efficiency (RE)" was defined as $RE = \frac{A}{A_0}$ to quantify the recycling efficiency of the SNA conjugates from two SNA assembly systems, where A_0 and A denote the initial absorbance value of system I (1.75) and the absorbance value of the recycled SNA solution, respectively. After calculation, the value of RE for the SNA conjugates was still as high as 0.824 after three recycling times (Figure S20). This strategy thus provides a facile way to recycle waste SNA conjugates in an SNA assembly system at constant temperature to save materials and costs.

CONCLUSIONS

In summary, we developed a detachable DNA circuit by embedding a pH-responsive intermolecular CG-C^+ triplex DNA structure between the toehold and branch migration domain of the DNA substrate. The intermolecular triplex structure only serves as a reversible connector to activate or inhibit the toehold and does not participate in the TMSDR process. The TMSDR rate is pH-dependent, and the "off/on" state of the detachable DNA circuit can be programmed by dynamic pH changes. Compared with a previous allosteric toehold strategy[20] and the intramolecular conformational motion strategy,[21] our strategy demonstrates a more facile

https://dx.doi.org/10.1021/acsnano.0c02329
ACS Nano 2020, 14, 8317−8327

regulation of the TMSDR through pH-controlled toehold activation or inhibition without introducing new DNA strands. A pH-controlled two-input DNA circuit composed of three DNA modules was then constructed by integrating the CG-C$^+$ triplex structure with the TA-T triplex structure to demonstrate the flexibility and adaptability of our strategy. In particular, a TMSDR-based resettable SNA assembly system was built through integrating the pH-controlled detachable DNA circuit with the self-assembly of SNAs. The SNA assembly system can be repeatedly operated six times with negligible loss of reactivity by cyclically varying the pH of the solution. Compared with previous renewable DNA devices that require extra reactants or thermal cyclers,[3,39,40] our system implements the complete reset of a TMSDR-based DNA device at constant temperature without generating additional waste DNA products. Moreover, this strategy provides an example to recycle waste SNA conjugates in an SNA assembly system to save materials and costs. Overall, the pH-controlled intermolecular triplex-based TMSDR strategy provides a facile and robust tool for the fields of dynamic DNA nanotechnology and DNA-mediated nanoparticle assembly. For example, this strategy should show great potential in building resettable large-scale integrated DNA networks and reprogrammable SNA assembly structures.

METHODS

Materials. All DNA oligonucleotides (Tables S1−S4) used in this work were designed by NUPACK software[59] to avoid any undesired secondary structures and then synthesized by Sangon Biotechnology Co., Ltd. (Shanghai, China). The 10 nm citrate-capped AuNPs used in the experiments were obtained from nanoComposix (San Diego, CA, USA). Tris(2-carboxyethyl)phosphine hydrochloride (TCEP) was obtained from Alfa Aesar. 4S GelRed was obtained from Sangon Biotechnology Co., Ltd. (Shanghai, China). Fetal bovine serum was ordered from Hyclone. Other chemicals were purchased from Sinopharm Chemical Reagent Co., Ltd. (China) unless otherwise indicated. Ultrapure water (18.2 MΩ·cm) (Millipore Co., USA) was used in all the experiments.

Buffer Conditions. For the experiments involving a pH-controlled DNA circuit system in solution, all DNA oligonucleotides were suspended in 1× Tris/EDTA/Mg^{2+} buffer (40 mM Tris, 1 mM EDTA, 12.5 mM $MgCl_2$, pH = 7.0). For the experiments involving assembly of SNAs, all DNA oligonucleotides except the thiol-terminated oligonucleotides were dissolved in 0.5 M phosphate-buffered saline (PBS, 0.5 M NaCl, 10 mM sodium phosphate, pH = 7.0). All reaction buffers with different pH values were adjusted by addition of small aliquots of 0.5 M HCl or 0.5 M NaOH.

Preparation of DNA Complexes. All oligonucleotides were purified *via* 10% denaturing PAGE (7 M urea, 1× Tris/boric acid/EDTA (TBE)) at first. Then, concentrations of all oligonucleotides were quantified by measuring the absorbance at 260 nm on a UV−vis spectrophotometer (Agilent, Cary 300, USA). Typically, a DNA complex (*e.g.*, S1-P) was prepared by mixing two complementary DNA strands at a molar ratio of 1:1; then the sample was kept at 95 °C for 5 min and slowly cooled to 25 °C at a rate of 0.1 °C/s. The hairpin structure (*e.g.*, S3) was also obtained using the same thermal annealing method. All prepared DNA samples were stored at 4 °C for further use.

Preparation of SNA. SNA was prepared according to the procedures in previous reports.[44,58] Thiol-terminated oligonucleotides were mixed with 100 mM TCEP for 1 h for the reduction reaction, then excess TCEP was removed *via* a NAP-5 column (GE Healthcare). Activated thiolated oligonucleotides were added to the AuNP solution in a molar ratio of ∼320:1 and incubated at 4 °C. After overnight incubation, the final concentrations of 0.01% sodium dodecyl sulfate (SDS) and 10 mM sodium phosphate (PB, pH = 7.0) were added to the solution, respectively. Then, a "salt aging" process was performed by gradually adding 5 M NaCl over 2 days. The solution was allowed to equilibrate overnight to reach the maximum DNA load after the final salt concentration up to 0.5 M NaCl. Unbound DNA strands were removed by three centrifugations (13 500 rpm, 60 min), and the precipitate was resuspended in 0.1 M PBS buffer (0.1 M NaCl, 10 mM sodium phosphate, pH = 7.0) and stored at 4 °C for further use. The concentration of SNA was determined by measuring the absorbance at 520 nm on an Agilent Cary 300 UV−vis spectrophotometer.

Preparation of DNA-Functionalized SNA (SNA-S2). SNA-S2 was prepared by mixing the S2 strands with SNA at different molar ratios, then heating to 45 °C for 5 min and slowly cooling to room temperature to ensure that the S2 strands were fully hybridized onto SNA. The solution was centrifuged at 13 500 rpm for 60 min to remove excess S2. Finally, the obtained SNA-S2 was resuspended in 0.5 M PBS (pH = 7.0) for further use.

Native PAGE Characterization. A running buffer of 1× TE/Mg^{2+} (40 mM Tris, 1 mM EDTA, 12.5 mM $MgCl_2$, adjusted to pH 5.5 and pH 7.0, respectively) was used here. All samples were incubated at 37 °C for 2 h in 1× TE/Mg^{2+} buffer (pH 5.5 or 7.0). Then, 12% native PAGE gel was run on a Tanon electrophoresis unit with a constant voltage of 110 V at 4 °C after DNA samples were loaded into wells.

Fluorescence Kinetic Measurements. All fluorescence kinetic measurements were performed by a fluorescence spectrophotometer (F-7000, Hitachi) at 37 °C after addition of different concentrations of reactants into a 200 μL cuvette. The excitation/emission was set at 645 nm/665 nm for kinetic characterization with the use of the Cy5 fluorophore.

Real-Time Monitoring of the SNA Assembly. The kinetics of the SNA assembly process was monitored by an Agilent Cary 300 UV−vis spectrophotometer at 37 °C. Typically, all reactants (20 nM SNA-S2, 2 μM S1-P, and different concentrations of input) were mixed in 0.5 M PBS buffer containing 0.01% SDS (SDS helps stabilize nanoparticles at high salt concentrations); the total volume for each sample was 120 μL. Then, the mixtures were slightly vortexed into a homogeneous solution and transferred to the cuvette of the UV−vis spectrophotometer. Finally, the SNA assembly process was detected by tracking the absorption of the sample at 520 nm.

Typical Operation for the Resettable SNA Assembly. Typically, 20 nM SNA-S2, 2 μM S1-P, and 6 μM input were added in a 0.5 M PBS buffer (pH = 5.5) containing 0.01% SDS to bring a total volume of 60 μL in a 200 μL PCR tube. The mixture was slightly vortexed into a homogeneous solution and incubated for 12 h at 37 °C in a metal bath for reaction. Then, the PCR tube was taken out for taking photos by a cell phone. Afterward, a small aliquot of 0.5 M NaOH was added into the solution to tune the pH to 7.0 for the SNA disassembly reaction. The disassembled sample was kept at 37 °C for 1 h after vortexing and centrifuged for 10 s at 4000 rpm. After taking a photo, the pH of the sample was changed to 5.5 by adding a small aliquot of 0.5 M HCl to proceed to the next round of the SNA assembly reaction. The same operation was repeated several times to study the resettable ability of the SNA assembly system.

Typical Operation for Recycling of SNA. First, all reactants of system I (20 nM SNA-S2, 2 μM S1-P, 6 μM input) were added in a 0.5 M PBS buffer (pH = 5.5, containing 0.01% SDS) to make a total reaction volume of 60 μL. Then, the mixture was incubated at 37 °C for the SNA assembly reaction. After 12 h of reaction, the sample was taken out for taking photos. Then, the pH of the sample was tuned to 7.0 to obtain a redispersed SNA solution of system I. After taking photos again, the sample was washed three times by centrifugation (13 500 rpm, 60 min) at 37 °C to remove all waste DNA strands, and the recycled SNA sample (SNA-S2) was resuspended in 0.5 M PBS buffer (pH = 5.5, containing 0.01% SDS). Then, the recycled SNA-S2 was reused in system II (composed of 20 nM recycled SNA-S2, 2 μM S1′-P′, 6 μM input′) under the same reaction conditions of system I. After 12 h of reaction at 37 °C, SNA-S2 was recycled from system II and reused for system I using the same operation as above.

https://dx.doi.org/10.1021/acsnano.0c02329
ACS Nano 2020, 14, 8317−8327

ASSOCIATED CONTENT

Supporting Information

The Supporting Information is available free of charge at https://pubs.acs.org/doi/10.1021/acsnano.0c02329.

Additional figures and tables (PDF)

Video S1: Rapid disassembly process of SNA aggregates after addition of small aliquots of NaOH (AVI)

AUTHOR INFORMATION

Corresponding Authors

Dongbao Yao − *CAS Key Laboratory of Soft Matter Chemistry, Collaborative Innovation Center of Chemistry for Energy Materials, Department of Polymer Science and Engineering, Hefei National Laboratory for Physical Sciences at the Microscale, University of Science and Technology of China, Hefei, Anhui 230026, People's Republic of China;* orcid.org/0000-0003-4719-9726; Email: dbyao@ustc.edu.cn

Haojun Liang − *CAS Key Laboratory of Soft Matter Chemistry, Collaborative Innovation Center of Chemistry for Energy Materials, Department of Polymer Science and Engineering, Hefei National Laboratory for Physical Sciences at the Microscale, University of Science and Technology of China, Hefei, Anhui 230026, People's Republic of China;* orcid.org/0000-0002-7840-7586; Email: hjliang@ustc.edu.cn

Authors

Yijun Guo − *CAS Key Laboratory of Soft Matter Chemistry, Collaborative Innovation Center of Chemistry for Energy Materials, Department of Polymer Science and Engineering, Hefei National Laboratory for Physical Sciences at the Microscale, University of Science and Technology of China, Hefei, Anhui 230026, People's Republic of China*

Bin Zheng − *School of Chemistry and Chemical Engineering, Hefei Normal University, Hefei, Anhui 230061, People's Republic of China*

Xianbao Sun − *CAS Key Laboratory of Soft Matter Chemistry, Collaborative Innovation Center of Chemistry for Energy Materials, Department of Polymer Science and Engineering, Hefei National Laboratory for Physical Sciences at the Microscale, University of Science and Technology of China, Hefei, Anhui 230026, People's Republic of China*

Xiang Zhou − *CAS Key Laboratory of Soft Matter Chemistry, Collaborative Innovation Center of Chemistry for Energy Materials, Department of Polymer Science and Engineering, Hefei National Laboratory for Physical Sciences at the Microscale, University of Science and Technology of China, Hefei, Anhui 230026, People's Republic of China*

Bing Wei − *CAS Key Laboratory of Soft Matter Chemistry, Collaborative Innovation Center of Chemistry for Energy Materials, Department of Polymer Science and Engineering, Hefei National Laboratory for Physical Sciences at the Microscale, University of Science and Technology of China, Hefei, Anhui 230026, People's Republic of China*

Shiyan Xiao − *CAS Key Laboratory of Soft Matter Chemistry, Collaborative Innovation Center of Chemistry for Energy Materials, Department of Polymer Science and Engineering, Hefei National Laboratory for Physical Sciences at the Microscale, University of Science and Technology of China, Hefei, Anhui 230026, People's Republic of China;* orcid.org/0000-0003-1159-1224

Miao He − *CAS Key Laboratory of Soft Matter Chemistry, Collaborative Innovation Center of Chemistry for Energy Materials, Department of Polymer Science and Engineering, Hefei National Laboratory for Physical Sciences at the Microscale, University of Science and Technology of China, Hefei, Anhui 230026, People's Republic of China*

Chengxu Li − *CAS Key Laboratory of Soft Matter Chemistry, Collaborative Innovation Center of Chemistry for Energy Materials, Department of Polymer Science and Engineering, Hefei National Laboratory for Physical Sciences at the Microscale, University of Science and Technology of China, Hefei, Anhui 230026, People's Republic of China*

Complete contact information is available at: https://pubs.acs.org/10.1021/acsnano.0c02329

Author Contributions

#Y.G. and D.Y. contributed equally to this work.

Notes

The authors declare no competing financial interest.

ACKNOWLEDGMENTS

We would like to thank the National Natural Science Foundation of China (Grant No. 21991132), the Fundamental Research Funds for the Central Universities (Grant No. WK2060200026), the Financial Grant from the China Postdoctoral Science Foundation (Grant No. 2018M630708), and the National Postdoctoral Program for Innovative Talents (Grant No. BX20180285) for their financial support. This work was additionally supported by the Foundations of Educational Committee of Anhui Province (Grant No. KJ2019A0719), the Excellent Talent Foundation of Education Department of Anhui Province (Grant No. gxyq2019066), and the 136 talent plan of Hefei Normal University.

REFERENCES

(1) Seeman, N. C. DNA in a Material World. *Nature* **2003**, *421*, 427−431.

(2) Seeman, N. C.; Sleiman, H. F. DNA Nanotechnology. *Nat. Rev. Mater.* **2018**, *3*, 17068.

(3) Yurke, B.; Turberfield, A. J.; Mills, A. P.; Simmel, F. C.; Neumann, J. L. A DNA-Fuelled Molecular Machine Made of DNA. *Nature* **2000**, *406*, 605−608.

(4) Zhang, D. Y.; Seelig, G. Dynamic DNA Nanotechnology Using Strand-Displacement Reactions. *Nat. Chem.* **2011**, *3*, 103−113.

(5) Scalise, D.; Schulman, R. Controlling Matter at the Molecular Scale with DNA Circuits. *Annu. Rev. Biomed. Eng.* **2019**, *21*, 469−493.

(6) Tian, Y.; Mao, C. Molecular Gears: A Pair of DNA Circles Continuously Rolls against Each Other. *J. Am. Chem. Soc.* **2004**, *126*, 11410−11411.

(7) Zhang, D. Y.; Turberfield, A. J.; Yurke, B.; Winfree, E. Engineering Entropy-Driven Reactions and Networks Catalyzed by DNA. *Science* **2007**, *318*, 1121−1125.

(8) Wu, C.; Cansiz, S.; Zhang, L.; Teng, I. T.; Qiu, L.; Li, J.; Liu, Y.; Zhou, C.; Hu, R.; Zhang, T.; Cui, C.; Cui, L.; Tan, W. A Nonenzymatic Hairpin DNA Cascade Reaction Provides High Signal Gain of mRNA Imaging inside Live Cells. *J. Am. Chem. Soc.* **2015**, *137*, 4900−4903.

(9) Qian, L.; Winfree, E. Scaling up Digital Circuit Computation with DNA Strand Displacement Cascades. *Science* **2011**, *332*, 1196−1201.

(10) Qian, L.; Winfree, E.; Bruck, J. Neural Network Computation with DNA Strand Displacement Cascades. *Nature* **2011**, *475*, 368−372.

(11) Yin, P.; Choi, H. M. T.; Calvert, C. R.; Pierce, N. A. Programming Biomolecular Self-Assembly Pathways. *Nature* **2008**, *451*, 318−322.

(12) Jung, C.; Allen, P. B.; Ellington, A. D. A Stochastic DNA Walker That Traverses a Microparticle Surface. *Nat. Nanotechnol.* **2016**, *11*, 157−163.
(13) Thubagere, A. J.; Li, W.; Johnson, R. F.; Chen, Z.; Doroudi, S.; Lee, Y. L.; Izatt, G.; Wittman, S.; Srinivas, N.; Woods, D.; Winfree, E.; Qian, L. A Cargo-Sorting DNA Robot. *Science* **2017**, *357*, No. eaan6558.
(14) Yao, D.; Bhadra, S.; Xiong, E.; Liang, H.; Ellington, A. D.; Jung, C. Dynamic Programming of a DNA Walker Controlled by Protons. *ACS Nano* **2020**, *14*, 4007−4013.
(15) Yao, D.; Song, T.; Sun, X.; Xiao, S.; Huang, F.; Liang, H. Integrating DNA-Strand-Displacement Circuitry with Self-Assembly of Spherical Nucleic Acids. *J. Am. Chem. Soc.* **2015**, *137*, 14107−14113.
(16) Srinivas, N.; Parkin, J.; Seelig, G.; Winfree, E.; Soloveichik, D. Enzyme-Free Nucleic Acid Dynamical Systems. *Science* **2017**, *358*, No. eaal2052.
(17) Chao, J.; Wang, J.; Wang, F.; Ouyang, X.; Kopperger, E.; Liu, H.; Li, Q.; Shi, J.; Wang, L.; Hu, J.; Wang, L.; Huang, W.; Simmel, F. C.; Fan, C. Solving Mazes with Single-Molecule DNA Navigators. *Nat. Mater.* **2019**, *18*, 273−279.
(18) Genot, A. J.; Zhang, D. Y.; Bath, J.; Turberfield, A. J. Remote Toehold: A Mechanism for Flexible Control of DNA Hybridization Kinetics. *J. Am. Chem. Soc.* **2011**, *133*, 2177−2182.
(19) Chen, X. Expanding the Rule Set of DNA Circuitry with Associative Toehold Activation. *J. Am. Chem. Soc.* **2012**, *134*, 263−271.
(20) Yang, X.; Tang, Y.; Traynor, S. M.; Li, F. Regulation of DNA Strand Displacement Using an Allosteric DNA Toehold. *J. Am. Chem. Soc.* **2016**, *138*, 14076−14082.
(21) Lai, W.; Ren, L.; Tang, Q.; Qu, X.; Li, J.; Wang, L.; Li, L.; Fan, C.; Pei, H. Programming Chemical Reaction Networks Using Intramolecular Conformational Motions of DNA. *ACS Nano* **2018**, *12*, 7093−7099.
(22) Idili, A.; Vallée-Bélisle, A.; Ricci, F. Programmable pH-Triggered DNA Nanoswitches. *J. Am. Chem. Soc.* **2014**, *136*, 5836−5839.
(23) Leitner, D.; Schröder, W.; Weisz, K. Influence of Sequence-Dependent Cytosine Protonation and Methylation on DNA Triplex Stability. *Biochemistry* **2000**, *39*, 5886−5892.
(24) Lu, C.-H.; Guo, W.; Hu, Y.; Qi, X.-J.; Willner, I. Multitriggered Shape-Memory Acrylamide−DNA Hydrogels. *J. Am. Chem. Soc.* **2015**, *137*, 15723−15731.
(25) Guo, W.; Lu, C.-H.; Orbach, R.; Wang, F.; Qi, X.-J.; Cecconello, A.; Seliktar, D.; Willner, I. pH-Stimulated DNA Hydrogels Exhibiting Shape-Memory Properties. *Adv. Mater.* **2015**, *27*, 73−78.
(26) Chen, X.; Chen, T.; Ren, L.; Chen, G.; Gao, X.; Li, G.; Zhu, X. Triplex DNA Nanoswitch for pH-Sensitive Release of Multiple Cancer Drugs. *ACS Nano* **2019**, *13*, 7333−7344.
(27) Amodio, A.; Adedeji, A. F.; Castronovo, M.; Franco, E.; Ricci, F. pH-Controlled Assembly of DNA Tiles. *J. Am. Chem. Soc.* **2016**, *138*, 12735−12738.
(28) Yao, D.; Li, H.; Guo, Y.; Zhou, X.; Xiao, S.; Liang, H. A pH-Responsive DNA Nanomachine-Controlled Catalytic Assembly of Gold Nanoparticles. *Chem. Commun.* **2016**, *52*, 7556−7559.
(29) Li, Y.; Song, L.; Wang, B.; He, J.; Li, Y.; Deng, Z.; Mao, C. Universal pH-Responsive and Metal-Ion-Free Self-Assembly of DNA Nanostructures. *Angew. Chem., Int. Ed.* **2018**, *57*, 6892−6895.
(30) Hu, Y.; Ren, J.; Lu, C.-H.; Willner, I. Programmed pH-Driven Reversible Association and Dissociation of Interconnected Circular DNA Dimer Nanostructures. *Nano Lett.* **2016**, *16*, 4590−4594.
(31) Sun, X.; Wei, B.; Guo, Y.; Xiao, S.; Li, X.; Yao, D.; Yin, X.; Liu, S.; Liang, H. A Scalable "Junction Substrate" to Engineer Robust DNA Circuits. *J. Am. Chem. Soc.* **2018**, *140*, 9979−9985.
(32) Amodio, A.; Zhao, B.; Porchetta, A.; Idili, A.; Castronovo, M.; Fan, C.; Ricci, F. Rational Design of pH-Controlled DNA Strand Displacement. *J. Am. Chem. Soc.* **2014**, *136*, 16469−16472.
(33) Zhang, D. Y.; Winfree, E. Control of DNA Strand Displacement Kinetics Using Toehold Exchange. *J. Am. Chem. Soc.* **2009**, *131*, 17303−17314.
(34) Zhang, D. Y. Cooperative Hybridization of Oligonucleotides. *J. Am. Chem. Soc.* **2011**, *133*, 1077−1086.
(35) Thubagere, A. J.; Thachuk, C.; Berleant, J.; Johnson, R. F.; Ardelean, D. A.; Cherry, K. M.; Qian, L. Compiler-Aided Systematic Construction of Large-Scale DNA Strand Displacement Circuits Using Unpurified Components. *Nat. Commun.* **2017**, *8*, 14373.
(36) Wang, F.; Lv, H.; Li, Q.; Li, J.; Zhang, X.; Shi, J.; Wang, L.; Fan, C. Implementing Digital Computing with DNA-Based Switching Circuits. *Nat. Commun.* **2020**, *11*, 121.
(37) Chang, X.; Zhang, C.; Lv, C.; Sun, Y.; Zhang, M.; Zhao, Y.; Yang, L.; Han, D.; Tan, W. Construction of a Multiple-Aptamer-Based DNA Logic Device on Live Cell Membranes *via* Associative Toehold Activation for Accurate Cancer Cell Identification. *J. Am. Chem. Soc.* **2019**, *141*, 12738−12743.
(38) Tomov, T. E.; Tsukanov, R.; Glick, Y.; Berger, Y.; Liber, M.; Avrahami, D.; Gerber, D.; Nir, E. DNA Bipedal Motor Achieves a Large Number of Steps Due to Operation Using Microfluidics-Based Interface. *ACS Nano* **2017**, *11*, 4002−4008.
(39) Garg, S.; Shah, S.; Bui, H.; Song, T.; Mokhtar, R.; Reif, J. Renewable Time-Responsive DNA Circuits. *Small* **2018**, *14*, 1801470.
(40) Hahn, J.; Shih, W. M. Thermal Cycling of DNA Devices *via* Associative Strand Displacement. *Nucleic Acids Res.* **2019**, *47*, 10968−10975.
(41) Cutler, J. I.; Auyeung, E.; Mirkin, C. A. Spherical Nucleic Acids. *J. Am. Chem. Soc.* **2012**, *134*, 1376−1391.
(42) Mirkin, C. A.; Letsinger, R. L.; Mucic, R. C.; Storhoff, J. J. A DNA-Based Method for Rationally Assembling Nanoparticles into Macroscopic Materials. *Nature* **1996**, *382*, 607−609.
(43) Park, S. Y.; Lytton-Jean, A. K. R.; Lee, B.; Weigand, S.; Schatz, G. C.; Mirkin, C. A. DNA-Programmable Nanoparticle Crystallization. *Nature* **2008**, *451*, 553−556.
(44) Macfarlane, R. J.; Lee, B.; Jones, M. R.; Harris, N.; Schatz, G. C.; Mirkin, C. A. Nanoparticle Superlattice Engineering with DNA. *Science* **2011**, *334*, 204−208.
(45) Laramy, C. R.; O'Brien, M. N.; Mirkin, C. A. Crystal Engineering with DNA. *Nat. Rev. Mater.* **2019**, *4*, 201−224.
(46) Zhou, X.; Yao, D.; Hua, W.; Huang, N.; Chen, X.; Li, L.; He, M.; Zhang, Y.; Guo, Y.; Xiao, S.; Bian, F.; Liang, H. Programming Colloidal Bonding Using DNA Strand-Displacement Circuitry. *Proc. Natl. Acad. Sci. U. S. A.* **2020**, *117*, 5617−5623.
(47) He, X.; Zeng, T.; Li, Z.; Wang, G.; Ma, N. Catalytic Molecular Imaging of MicroRNA in Living Cells by DNA-Programmed Nanoparticle Disassembly. *Angew. Chem., Int. Ed.* **2016**, *55*, 3073−3076.
(48) Liang, C.-P.; Ma, P.-Q.; Liu, H.; Guo, X.; Yin, B.-C.; Ye, B.-C. Rational Engineering of a Dynamic, Entropy-Driven DNA Nanomachine for Intracellular MicroRNA Imaging. *Angew. Chem., Int. Ed.* **2017**, *56*, 9077−9081.
(49) Liu, J.; Lu, Y. A Colorimetric Lead Biosensor Using Dnazyme-Directed Assembly of Gold Nanoparticles. *J. Am. Chem. Soc.* **2003**, *125*, 6642−6643.
(50) Kato, D.; Oishi, M. Ultrasensitive Detection of DNA and RNA Based on Enzyme-Free Click Chemical Ligation Chain Reaction on Dispersed Gold Nanoparticles. *ACS Nano* **2014**, *8*, 9988−9997.
(51) Wei, B.; Yao, D.; Zheng, B.; Zhou, X.; Guo, Y.; Li, X.; Li, C.; Xiao, S.; Liang, H. Facile Strategy for Visible Disassembly of Spherical Nucleic Acids Programmed by Catalytic DNA Circuits. *ACS Appl. Mater. Interfaces* **2019**, *11*, 19724−19733.
(52) Li, X.; Yao, D.; Zhou, J.; Zhou, X.; Sun, X.; Wei, B.; Li, C.; Zheng, B.; Liang, H. Cascaded DNA Circuits-Programmed Self-Assembly of Spherical Nucleic Acids for High Signal Amplification. *Sci. China Chem.* **2020**, *63*, 92−98.
(53) Zhao, Z.; Chen, C.; Dong, Y.; Yang, Z.; Fan, Q.-H.; Liu, D. Thermally Triggered Frame-Guided Assembly. *Angew. Chem., Int. Ed.* **2014**, *53*, 13468−13470.

https://dx.doi.org/10.1021/acsnano.0c02329
ACS Nano 2020, 14, 8317−8327

(54) Ohta, S.; Glancy, D.; Chan, W. C. W. DNA-Controlled Dynamic Colloidal Nanoparticle Systems for Mediating Cellular Interaction. *Science* **2016**, *351*, 841−845.
(55) Li, H.; Zhou, X.; Yao, D.; Liang, H. pH-Responsive Spherical Nucleic Acid for Intracellular Lysosome Imaging and an Effective Drug Delivery System. *Chem. Commun.* **2018**, *54*, 3520−3523.
(56) Song, T.; Xiao, S.; Yao, D.; Huang, F.; Hu, M.; Liang, H. An Efficient DNA-Fueled Molecular Machine for the Discrimination of Single-Base Changes. *Adv. Mater.* **2014**, *26*, 6181−6185.
(57) Li, Y.; Wang, G. A.; Mason, S. D.; Yang, X.; Yu, Z.; Tang, Y.; Li, F. Simulation-Guided Engineering of an Enzyme-Powered Three Dimensional DNA Nanomachine for Discriminating Single Nucleotide Variants. *Chem. Sci.* **2018**, *9*, 6434−6439.
(58) Jin, R.; Wu, G.; Li, Z.; Mirkin, C. A.; Schatz, G. C. What Controls the Melting Properties of DNA-Linked Gold Nanoparticle Assemblies? *J. Am. Chem. Soc.* **2003**, *125*, 1643−1654.
(59) Zadeh, J. N.; Steenberg, C. D.; Bois, J. S.; Wolfe, B. R.; Pierce, M. B.; Khan, A. R.; Dirks, R. M.; Pierce, N. A. Nupack: Analysis and Design of Nucleic Acid Systems. *J. Comput. Chem.* **2011**, *32*, 170−173.

https://dx.doi.org/10.1021/acsnano.0c02329
ACS Nano 2020, 14, 8317−8327